

Article

Aliphatic-Bridged Early Lanthanide Metal–Organic Frameworks: Topological Polymorphism and Excitation-Dependent Luminescence

Pavel A. Demakov , Alexey A. Ryadun and Vladimir P. Fedin * 

Nikolaev Institute of Inorganic Chemistry SB RAS, 3 Lavrentiev Ave., 630090 Novosibirsk, Russia

* Correspondence: cluster@niic.nsc.ru

Abstract: Six new three-dimensional metal–organic frameworks based on early lanthanide(III) cations and *trans*-1,4-cyclohexanedicarboxylic acid (H₂chdc) were obtained. Their crystal structures were determined by single-crystal X-ray diffraction analysis. The structure of [La₂(H₂O)₄(chdc)₃]·2DMF·H₂O (**1**; DMF = N,N-dimethylformamide) contains one-dimensional infinite La(III)-carboxylate chains interconnected by cyclohexane moieties to form a highly porous polymeric lattice with 30% solvent accessible volume. Compounds [Ln₂(phen)₂(chdc)₃]·0.75DMF (**2**_{Ln}; Ln³⁺ = Ce³⁺, Pr³⁺, Nd³⁺ and Sm³⁺; phen = 1,10-phenanthroline) are based on binuclear carboxylate building blocks, which are decorated by chelate phenanthroline ligands and interconnected by cyclohexane moieties to form more dense isostructural coordination frameworks with primitive cubic *pcu* topology. Compound [Nd₂(phen)₂(chdc)₃]·2DMF·0.67H₂O (**3**) is based on secondary building units similar to **2**_{Ln} and contains a coordination lattice isomeric to **2**_{Ln} with a rare hexagonal helical *szz* topology. Thermal stability and luminescent properties were investigated. For **2**_{Sm}, a strong and nonmonotonous dependence of the luminescence color on the variation of excitation wavelength was revealed, changing its emission from pinkish red at λ_{ex} = 340 nm to white at λ_{ex} = 400 nm, and then to yellow at lower excitation energies. Such nonlinear behavior was rationalized in terms of the contribution of several different luminescence mechanisms. Thus, **2**_{Sm} is a rather rare example of a highly tunable monometallic lanthanide-based luminophore with possible applications in light-emitting devices and optical data processing.

Keywords: coordination polymers; metal–organic frameworks; polymorphism; rare earth elements; luminescence



Citation: Demakov, P.A.; Ryadun, A.A.; Fedin, V.P. Aliphatic-Bridged Early Lanthanide Metal–Organic Frameworks: Topological Polymorphism and Excitation-Dependent Luminescence. *Inorganics* **2022**, *10*, 163. <https://doi.org/10.3390/inorganics10100163>

Academic Editor: Alexander Artem'ev

Received: 30 August 2022

Accepted: 26 September 2022

Published: 1 October 2022

Publisher's Note: MDPI stays neutral with regard to jurisdictional claims in published maps and institutional affiliations.



Copyright: © 2022 by the authors. Licensee MDPI, Basel, Switzerland. This article is an open access article distributed under the terms and conditions of the Creative Commons Attribution (CC BY) license (<https://creativecommons.org/licenses/by/4.0/>).

1. Introduction

Metal–organic frameworks (MOFs) represent an emerging class of hybrid inorganic–organic materials. A design of diverse functional properties, e.g., catalytic, optical, adsorption and magnetic, is possible in MOFs by carefully choosing metal building blocks and organic bridges [1–6]. The effects of reversible structural transitions (breathing) [7–10] and topological polymorphisms [11–13] inherent to metal–organic coordination polymers are of great interest due to the corresponding ability of fine tuning the porosity, crystal packing of functional centers and strength of host–guest interactions. The aliphatic-backboned ligands bearing their own enhanced structural mobility and specific optical, thermal and adsorption properties [14–17] deserve special attention in MOF chemistry. In particular, the optical transparency of such ligands gives us the perfect ability to investigate the photophysical properties of photoactive coordination nodes or guest molecules incorporated into the aliphatic-spread polymeric network [18,19].

Lanthanide-based metal–organic frameworks are extensively studied owing to their remarkable luminescence [20–23] originating from the emission of metal cation when organic ligands and guest molecules with conjugated π-systems often act as photosensitizers for self-emitting Ln³⁺. In particular, combining lanthanide(III) ions bearing different emission

colors and/or using highly emissive organic guests or ligands within Ln^{3+} -based MOFs is a convenient route for the synthesis of single-phase white-light emitters suitable for real applications [24–29]. High coordination numbers of $\text{Ln}(\text{III})$ ions and the corresponding abundant structural variability of polymeric coordination lattices [30–32] push ahead their synthesis and comprehensive investigations. Ln^{3+} -based MOFs are also characterized by higher thermal and hydrolytic stabilities compared to more common frameworks based on divalent transition metal cations [33–35], which makes them suitable for applications in sensor devices, light emitters and bioimaging [36–40].

Previously, we have reported a series of metal–organic frameworks based on 1,10-phenanthroline (phen) and *trans*-1,4-cyclohexanedicarboxylic acid (H_2chdc) with the formulas $[\text{Ln}_2(\text{phen})_2(\text{chdc})_3] \cdot 0.5\text{DMF}$ ($\text{Ln}^{3+} = \text{Eu}^{3+}, \text{Gd}^{3+}, \text{Tb}^{3+}, \text{Y}^{3+}$) [28,41], for which a strong and excitation wavelength-dependent luminescence with quantum yields of up to 63% was observed. The origin of luminescence varied from metal-centered antenna-sensitized emission for Eu^{3+} and Tb^{3+} compounds to the ligand-centered emission for the compounds with non-emissive Gd^{3+} or Y^{3+} cations. Tuning the metal coordination environment by nitrate, chloride or carboxylate in a series of structurally kindred $\text{Gd}(\text{III})$ metal–organic frameworks with an optically transparent *trans*-1,4-cyclohexanedicarboxylate bridge allowed us to understand the impact of the coordinated X anion on the ligand-centered luminescence in photoactive $\{\text{Gd}_2(\text{phen})_2(\text{X})_2(\text{OOCR})_4\}$ moiety. Owing to the intensive and highly tunable luminescence of several MOFs of the $[\text{Ln}_2(\text{phen})_2(\text{chdc})_3]$ family, we further focused on the synthesis and investigation of $[\text{Ln}_2(\text{phen})_2(\text{chdc})_3]$ -type metal–organic frameworks with early lanthanides based on an isostructural binuclear carboxylate building block (Figure 1). Early Ln^{3+} cations are also known to have unique emission characteristics. As a result, this work reports the successful isolation and characterization of six new MOFs constructed by early lanthanides and H_2chdc with the corresponding crystallographic formulae $[\text{La}_2(\text{H}_2\text{O})_4(\text{chdc})_3] \cdot 2\text{DMF} \cdot \text{H}_2\text{O}$ (**1**; DMF = *N,N*-dimethylformamide), $[\text{Ln}_2(\text{phen})_2(\text{chdc})_3] \cdot 0.75\text{DMF}$ (**2_{Ln}**; $\text{Ln}^{3+} = \text{Ce}^{3+}, \text{Pr}^{3+}, \text{Nd}^{3+}$ and Sm^{3+}) and $[\text{Nd}_2(\text{phen})_2(\text{chdc})_3] \cdot 2\text{DMF} \cdot 0.67\text{H}_2\text{O}$ (**3**). The numbers 1–3 represent different structural types inherent to the compounds obtained in close conditions. A non-photosensitized luminescence was revealed for **2_{Nd}**, while **2_{Sm}** demonstrated strongly excitation-dependent color of emission, which is rather unusual for monometallic $\text{Ln}(\text{III})$ metal–organic frameworks.

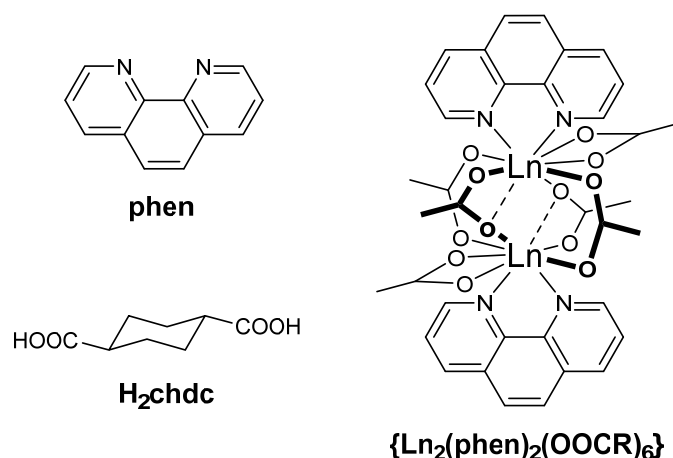


Figure 1. Structural formulae of the used ligands and secondary building unit in **2_{Ln}**.

2. Results and Discussion

2.1. Synthesis

Single crystals of compound $[\text{La}_2(\text{H}_2\text{O})_4(\text{chdc})_3] \cdot 2\text{DMF} \cdot \text{H}_2\text{O}$ (**1**) were obtained by the reaction between lanthanum(III) chloride, *trans*-1,4-cyclohexanedicarboxylic acid (H_2chdc) and 1,10-phenanthroline (phen) in a mixture of *N,N*-dimethylformamide (DMF) and water at 80 °C. Phenanthroline is not comprised in **1**; however, carrying the reaction without

phen in similar conditions resulted in the formation of an unidentified crystalline phase. The role of 1,10-phenanthroline in the synthesis could be suggested in terms of its slight basicity [42,43], promoting the deprotonation of weak organic acid H_2chdc . The PXRD pattern of the filtered sample of **1'** shows its poor crystallinity, which might be attributed to the mobility of highly porous coordination framework based on conformationally flexible $chdc$ ligand after removal of the mother liquor and subsequent desolvation of **1** (see pages 10–12 in ESI). Chemical analysis of **1'** samples after the storage (see Section 3.3 in the experimental) confirms the substantial decrease in guest molecule content, compared to the crystallographic formula of **1**.

Compounds $[Ln_2(phen)_2(chdc)_3] \cdot 0.75DMF$ (2_{Ln} ; $Ln^{3+} = Ce^{3+}, Pr^{3+}, Nd^{3+}$ and Sm^{3+}) were synthesized in conditions quite similar to **1**, except for changing lanthanum(III) chloride to the corresponding amounts of other lanthanide(III) salts and some variation in solvent DMF: H_2O ratio. This synthetic method was optimized to avoid the formation of unidentified crystalline phases. PXRD patterns of 2_{Ln} (Figures S1–S4) correspond well to the theoretical ones, indicating their successful synthesis. Unlike **1**, crystal structures of 2_{Ln} contain a phen molecule being coordinated to each Ln(III) ion. Such difference between La-based **1** and compounds 2_{Ln} is apparently attributed to the widely known effect on the decrease in the atomic and ionic radii in the lanthanide row with increasing atomic number (called lanthanide contraction), which results in the possible chemical and structural dissimilarity [30,44,45] of the forming coordination compounds; the latter is more comprehensively discussed in the next part.

Single crystals of $[Nd_2(phen)_2(chdc)_3] \cdot 2DMF \cdot 0.67H_2O$ (**3**) were obtained in low yield by the reaction of neodymium(III) chloride, H_2chdc and phen in DMF at $110^\circ C$. The formation of **3** appears to compete strongly to the crystallization of 2_{Nd} . Time screening at $110^\circ C$ revealed that **3** crystallizes as a major product only during several hours of heating (Figure 2), while increasing the synthesis time up to two days carrying all other similar conditions leads to pure 2_{Nd} precipitation. In this regard, **3** can be recognized as a metastable kinetic reaction product. Temperature screening at a short synthesis time showed that **3** forms as only a minor admixture to 2_{Nd} at $120^\circ C$, while no precipitation was observed at $100^\circ C$ and $130^\circ C$. Surprisingly, no formation of **3**-like phases was observed in similar screening syntheses using Pr(III) and Sm(III) (Figures S5 and S6), which are the nearest available neighbors of neodymium in the lanthanide row, which puts Nd-based **3**, topologically isomeric to the 2_{Nd} coordination framework, in a completely unique place.

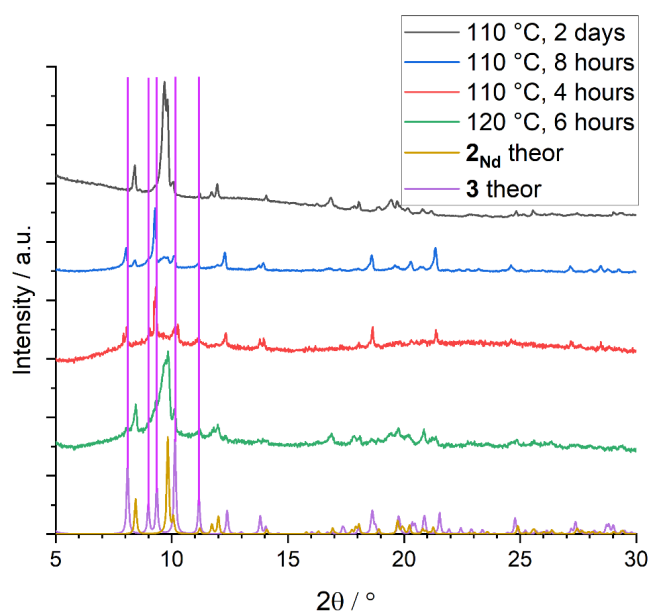


Figure 2. PXRD patterns for 2_{Nd} /**3** temperature- and time-screening syntheses. Magenta lines show positions for lowest-angle reflections from the theoretical **3** structure.

2.2. Crystal Structure Description

A suitable crystal of **1** was taken directly from the mother liquor before the filtration for performing single-crystal XRD. Compound **1** crystallizes in the triclinic symmetry with $P\bar{1}$ space group. The asymmetric unit of **1** includes one La atom. La(III) is coordinated by two O atoms of two κ^2 -carboxylic groups, four O atoms of two chelated κ^2, κ^1 -carboxylic groups, two O atoms of two nonchelated κ^2, κ^1 -carboxylic groups and two O atoms of two water molecules. Therefore, the La atom adopts the coordination number 10. La–O(COO) bond lengths range from 2.524(3) Å to 2.771(3) Å and La–O(H₂O) bond lengths are 2.525(3) Å and 2.543(3) Å. La atoms are interconnected by κ^2, κ^1 -carboxylate bridges forming one-dimensional $\{-\text{La}(\text{OH}_2)_2(\text{OOCR})_3\}_n$ chains (Figure 3a), which act as building units in the coordination framework. These chains are interconnected by cyclohexane moieties to form a three-dimensional polymeric lattice, in which chdc ligands present in two different ($\kappa^2, \kappa^1; \kappa^2, \kappa^1$) and ($\kappa^2; \kappa^2$) coordination modes (Figure S7), situated along the b and c axes, respectively. The coordination framework in **1** contains the system of one-dimensional channels running in two perpendicular directions. The larger channels paved by cyclohexane rings (Figure 3b) are situated along the a crystallographic axis and are ca. 4×4 Å² in size (Figure S8a). The smaller channels paved by cyclohexane rings and coordinated water molecules (Figure 3c) are situated along the b crystallographic axis and are ca. 3×4 Å² in size (Figure S8b). These two types of channels intersect and the total solvent accessible volume in **1** reaches 30%. The channels are fully occupied by guest DMF and water molecules.

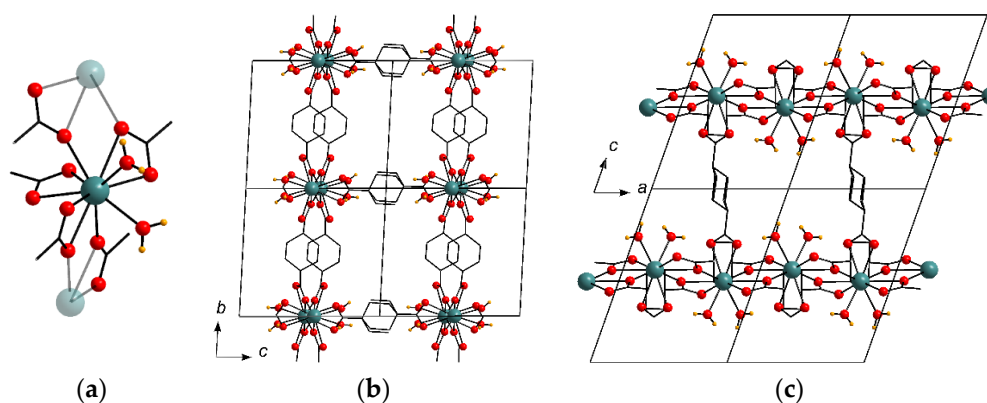


Figure 3. La(III) environment in **1**. The neighboring La(III) ions are shown as transparent. O atoms are red, H atoms are orange (a). View along different crystallographic axes in **1**: a (b) and b (c). Guest molecules and H atoms of chdc ligand are not shown. Only one possible position of disordered ($\kappa^2; \kappa^2$)-chdc cyclohexane ring is shown.

Compounds **2_{Ce}**, **2_{Pr}**, **2_{Nd}** and **2_{Sm}** were obtained under similar conditions and are isostructural. Therefore, only the **2_{Nd}** structure will be described in detail as a representing example, which is also may be conveniently compared to the **3_{Nd}** structure described below. **2_{Nd}** crystallizes in the monoclinic symmetry with the $P2_1/n$ space group. Nd(III) is coordinated by two O atoms of the κ^2 -carboxylic group, two O atoms of the chelated κ^2, κ^1 -carboxylic group, one O atom of the nonchelated κ^2, κ^1 -carboxylic group, two O atoms of two κ^1, κ^1 -carboxylic groups and two N atoms of the phenanthroline chelate molecule. Therefore, the Nd atom adopts the coordination number 9. The bond lengths of the metal coordination environment in **2_{Ln}** are presented in Table S3. Two symmetry-equivalent Nd atoms are coupled into binuclear $\{\text{Nd}_2(\text{phen})_2(\text{OOCR})_6\}$ building blocks (Figure 4a) acting as six connected nodes in the coordination framework. Importantly, the lanthanum-based **1** was obtained in conditions similar to **2_{Ln}**, including the addition of phenanthroline, despite the metal salt precursor. Therefore, a lanthanide contraction leads not only to the decrease in the metal coordination number from 10 (**1**) to 9 (**2_{Ln}**), but also to the coordination of phen instead of two water molecules and to the change in the structural type of the secondary

building unit from infinite 1D chains (**1**) to separate binuclear carboxylate blocks (2_{Ln}). These blocks are interconnected by cyclohexane moieties, forming a three-dimensional polymeric lattice (Figure 4b) with primitive cubic (*pcu*) topology (Figure 4c). As it was found by the PLATON routine [46], the voids in 2_{Nd} are represented by small isolated cages with only 6% total solvent accessible volume. These cages are filled by partially occupied guest DMF positions with 0.75DMF content per formula unit.

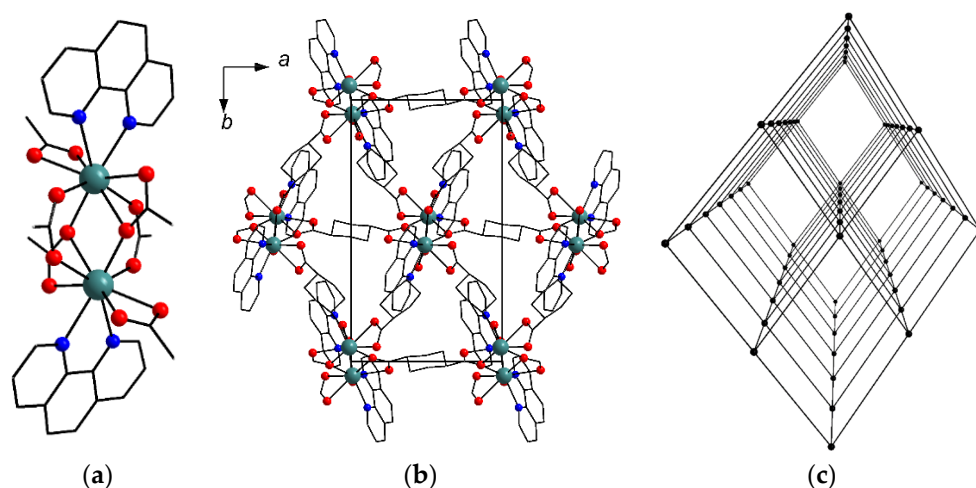


Figure 4. Binuclear block $\{Nd_2(phen)_2(OOCR)_6\}$ in the structure of 2_{Nd} (a) and view along *c* crystallographic axis (b). O atoms are red, N atoms are blue, H atoms and guest molecules are not shown. Topological representation of the coordination lattice in 2_{Nd} (c). Binuclear block $\{Nd_2(phen)_2(OOCR)_6\}$ is shown as a black node.

Compound **3** crystallizes in the trigonal symmetry with the *R*- $\bar{3}$ space group. The Nd(III) coordination environment and structure of the binuclear $\{Nd_2(phen)_2(OOCR)_6\}$ carboxylate block (Figure 5a) are similar to those in 2_{Nd} . However, the packing of such building units is different, which leads to the helical *snz* topology (Figure 5c) of a coordination lattice, rarely occurring in MOFs [47,48]. The framework in **3** contains one-dimensional channels running along *c* crystallographic axis (Figure 5b). These channels are paved by phenanthroline molecules and are ca. $4 \times 4 \text{ \AA}^2$ in size. The total solvent accessible volume in **3** is more than in 2_{Nd} and reaches 8%. The channels are fully occupied by guest DMF and water molecules.

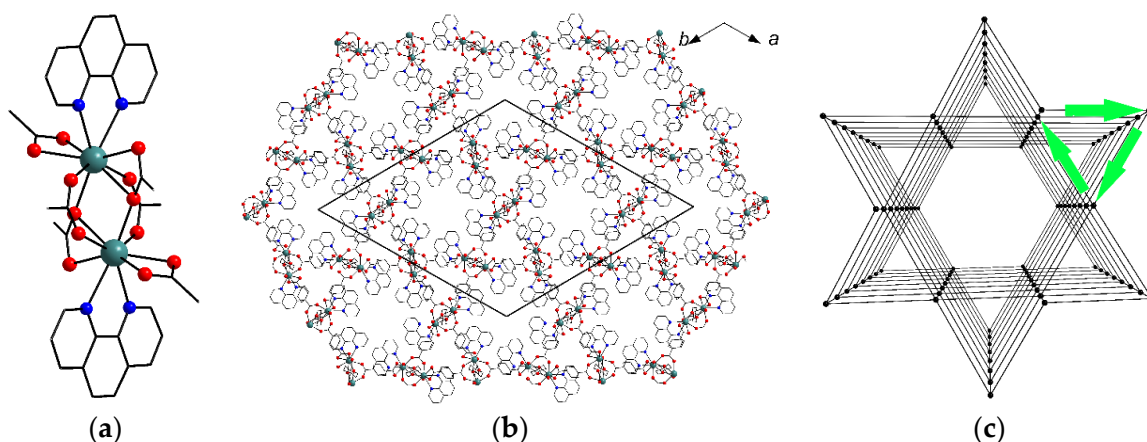


Figure 5. Binuclear block $\{Nd_2(phen)_2(OOCR)_6\}$ in the structure of **3** (a) and view along *c* crystallographic axis (b). Atom colors correspond to Figure 4; guest molecules are not shown. Topological representation of the coordination lattice in **3** (c). Binuclear block $\{Nd_2(phen)_2(OOCR)_6\}$ is shown as a black node. Green arrows show a helical structure of trilateral channels in the net.

2.3. Characterization and Thermal Properties

The crystal structure of **1** was found to be unstable after filtration. The PXRD pattern of the filtered sample shown in Figure S9a demonstrates a significant decrease in its crystallinity. The interpretation of chemical and physicochemical analyses performed for this sample, which is denoted as **1'**, is provided in pages 10–12 of the Supplementary Information file.

Infrared spectra (Figure S11) of the samples **2_{Ln}** correspond well to their compositions firstly determined by the single-crystal XRD. The spectra of **2_{Ln}** contain typical cyclohexane ring and DMF methyl group C(sp³)–H vibrations, DMF C=O vibrations and COO-group antisymmetric and symmetric stretchings. A presence of weak coupled bands at 3075–3060 cm⁻¹ corresponding to the valence vibrations of C(sp²)–H bonds, as well as strong bands at ca. 1583, 1534 and 850 cm⁻¹, belonging to the phenanthroline oscillations [49,50], prove the successful incorporation of the phen ligand into coordination frameworks **2_{Ln}** instead of **1**, fully consisting with their crystal structures. Elemental CHN and thermogravimetric data (Figure 6) also confirm the chemical nature and guest composition of the synthesized MOFs **2_{Ln}**. According to TGA, slow solvent loss occurs in the range of 250–450 °C; such a high temperature of guest DMF and water release is apparently attributed to their isolation into very narrow-windowed pores (see above). Decomposition of the coordination frameworks in **2_{Ln}** occurs at 470–510 °C, according to the temperatures of weight loss rate local maxima. Weights of final residues at 600 °C exceed the calculated weights of lanthanide oxides (Table S4), which indicates a presence of a considerable amount of carbon admixture in the thermolysis products of **2_{Ln}**, due to the incomplete evaporation of organic moieties. Such thermal stability fits typical values for the phenanthroline-coordinated carboxylate MOFs of early lanthanides [51–54].

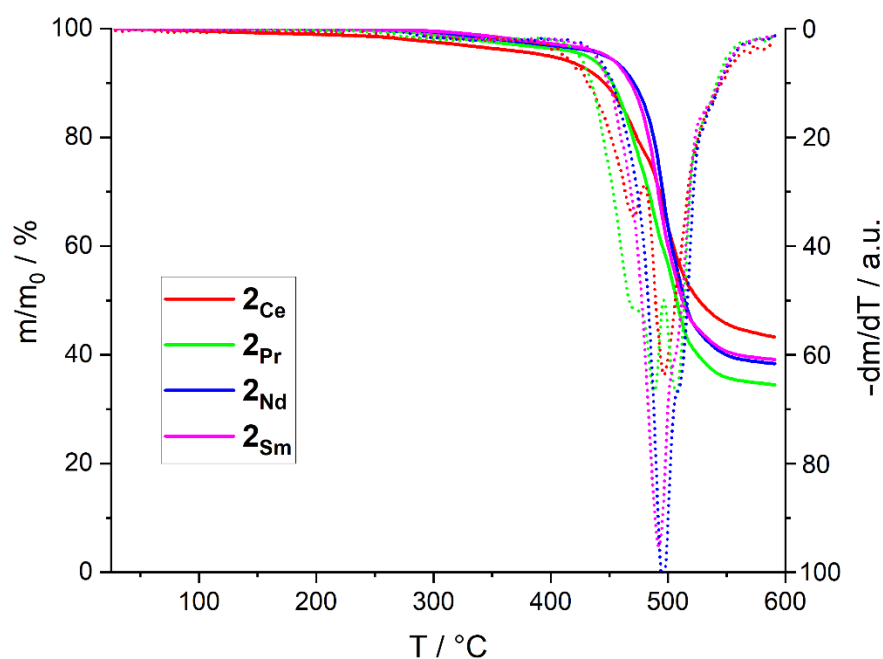


Figure 6. TG plots for compounds **1'**, **2_{Ln}** (solid) and relative dm/dT (dashed).

2.4. Luminescent Properties

As it was described in the introduction, a series of metal–organic frameworks with the formulae $[Ln_2(phen)_2(chdc)_3] \cdot 0.5DMF$ ($Ln^{3+} = Eu^{3+}, Gd^{3+}, Tb^{3+}, Y^{3+}$), in which the coordination lattice is isostructural to **2_{Ln}**, was reported by us previously. Highly effective and tunable luminescence was revealed for such series. Since that, the investigation of luminescent properties of **2_{Ln}**, especially for **2_{Sm}** containing a moderately emissive Sm^{3+} cation, has been of great interest. The luminescent measurements revealed no emission

for 2Ce and 2Pr , possibly due to the strong paramagnetic quenching of the corresponding cations. For 2Nd , a weak infrared emission with $\lambda_{\text{em}} = 1102$ nm was observed under 804 nm excitation (Figure S12). This emission band is attributed to the ${}^4\text{F}_{3/2} \rightarrow {}^4\text{I}_{11/2}$ transition in Nd^{3+} [55–57] and the excitation band might be attributed to the ${}^4\text{F}_{9/2} \rightarrow {}^4\text{I}_{11/2}$ transition [58,59] or to ${}^4\text{F}_{5/2}, {}^4\text{H}_{9/2} \rightarrow {}^4\text{I}_{9/2}$ transitions [60], indicating no apparent sensitization of Nd^{3+} luminescence by phenanthroline.

Solid-state luminescent properties of 2Sm were also investigated. The excitation spectrum is shown in Figure S13. The emission spectrum at $\lambda_{\text{ex}} = 340$ nm (Figure 7a) contains a wide several-moded band in the UV-violet region, apparently attributed to the phenanthroline ligand-centered emission, and a series of strong bands at $\lambda_{\text{em}} = 564$ nm, 598 nm and 646 nm, typical to the Sm^{3+} -centered emission and corresponding to the series of ${}^4\text{G}_{5/2} \rightarrow {}^6\text{H}_j$ ($j = 5/2, 7/2, 9/2$, respectively) transitions. The integral emission color of 2Sm at $\lambda_{\text{ex}} = 340$ nm is pinkish-red (Figure 7b), as is seen from the CIE 1931 chromaticity diagram. Sm^{3+} is known to be a mild energy acceptor in photosensitization processes, compared to Eu^{3+} , representing the strongest emitter among Ln(III) cations. Therefore, the emission of Sm^{3+} in its coordination complexes often competes to the intraligand emission of the coordinated photoactive species. In different MOF cases, Sm^{3+} emission may be either dominant [61–63] or almost silent [64–66], the latter indicating ineffective energy transfer to the metal ion from organic antenna. Moreover, the emission intensities of both Sm^{3+} and ligand components can be comparable to each other [67,68], which could unveil a route for a pronounced color tuning in a simple single-lanthanide system, which is preferable for real applications, although there are some reported nice examples of effective emission color tuning in Sm-MOFs by codoping with other lanthanides [64,69,70]. Since the emission of 2Sm belongs to the third of the types described above, and owing to the λ_{ex} dependence of emission color previously reported by us for close (Y/Eu/Tb)-phen-chdc systems [28], we decided to further study the luminescence of 2Sm in a wide range of excitation wavelengths.

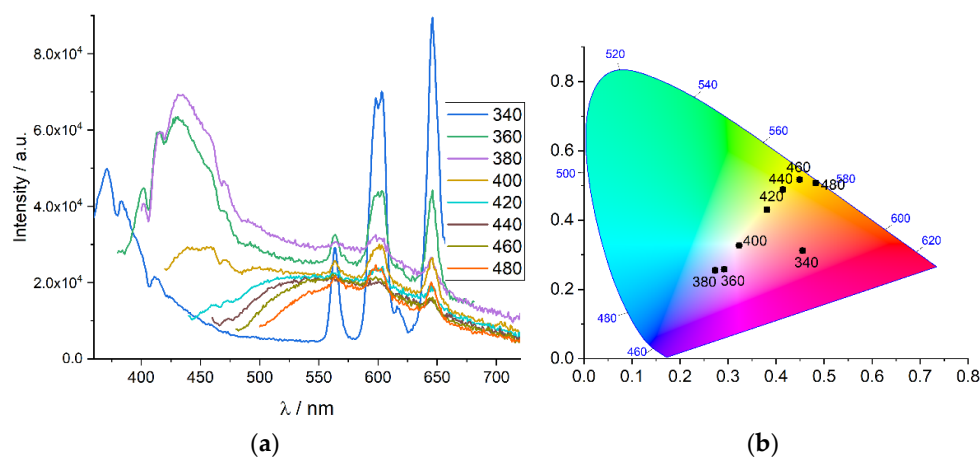


Figure 7. Emission spectra for 2Sm at different excitation wavelengths (a). CIE 1931 chromaticity diagram for 2Sm calculated from emission spectra (b).

The luminescent spectra for 2Sm under varying λ_{ex} are shown in Figure 7a. With an increase in the excitation wavelength from 340 nm to the higher wavelengths, a gradual red shift of phenanthroline emission band is observed, which may be due to the redistribution of the vibrational states of such a large conjugated system. Due to moving the main maximum of wide-banded emission from ca. 370 nm (UV region) to ca. 430 nm (visible region), the overall increase in blue color contribution is observed, as indicated by chromaticity diagram (Figure 7b). Further increasing the excitation wavelength leads to the weakening of blue emission bands, giving almost perfect white light at $\lambda_{\text{ex}} = 400$ nm with the corresponding (x,y) coordinates of (0.323,0.327). The correlated color temperature (CCT), which is calculated for this point to be 5970 K, and 5% color purity for the 480 nm blue characteristic wavelength, indicate an almost perfect daylight color suitable

for the implementation in WLEDs. A further decrease in the excitation energy leads to the complete vanishing of blue emission, while a relatively weak emission of Sm^{3+} is still retained even at $\lambda_{\text{ex}} = 480$ nm, which further results in a gradual shift of the emission color to the yellow region upon blue light excitation. Such a complex nonlinear variation of 2_{Sm} luminescence color is apparently attributed to the abovementioned competing between different luminescence mechanisms, including ligand-centered emission of the coordinated phenanthroline and dipole–dipole energy transfer from phen antenna to the emissive Sm^{3+} center. Although there are several reported examples of single-metal samarium MOF white emitters [71–74], no excitation-dependent color tuning was reported for Sm(III)-based carboxylate coordination compounds with any ligand containing 2,2'-bipyridyl cores, to the best of our knowledge. Therefore, 2_{Sm} is an unusual example of a pronounced tuning of the emission color in a monometallic lanthanide-based MOF, which makes it promising for obtaining multicolored luminophores and optical data processing.

3. Experimental

3.1. Materials

Trans-1,4-cyclohexanedicarboxylic acid (H_2chdc , >97.0%) and 1,10-phenanthroline monohydrate ($\text{phen}\cdot\text{H}_2\text{O}$, >98.0%) were received from TCI. *N,N*-dimethylformamide (DMF, reagent grade) was received from Vekton. Cerium(III) nitrate hexahydrate ($\text{Ce}(\text{NO}_3)_3\cdot 6\text{H}_2\text{O}$, 99.5% REO) was received from Alfa Aesar. Lanthanide(III) chloride hydrates ($\text{LaCl}_3\cdot 7\text{H}_2\text{O}$, high-purity grade; $\text{PrCl}_3\cdot 7\text{H}_2\text{O}$, high-purity grade; $\text{NdCl}_3\cdot 7\text{H}_2\text{O}$, high purity grade; $\text{SmCl}_3\cdot 6\text{H}_2\text{O}$, reagent grade) were received from Novosibirsk Rare Metals Plant. All reagents were used as received without further purification.

3.2. Instruments

IR spectra in KBr pellets were recorded in the range 4000–400 cm^{-1} on a Bruker Scimitar FTS 2000 spectrometer. Elemental analysis was conducted with a VarioMICROcube analyzer. Powder X-ray diffraction (PXRD) analysis was performed at room temperature on a Bruker D8 Advance diffractometer (Cu-K α radiation, $\lambda = 1.54178$ Å). Thermogravimetric analysis was carried out using a Netzsch TG 209 F1 Iris instrument under Ar flow (30 $\text{cm}^3\cdot\text{min}^{-1}$) at a 10 $\text{K}\cdot\text{min}^{-1}$ heating rate. Photoluminescence spectra were recorded with a spectrofluorometer Horiba Jobin Yvon Fluorolog 3 equipped with ozone-free Xe-lamp 450W power, cooled photon detector R928/1860 PFR technologies with refrigerated chamber PC177CE-010 and double-grating monochromators. The spectra were corrected for source intensity and detector spectral response by standard correction curves.

3.3. Synthetic Methods

Synthesis of 1. Amounts of 55.0 mg (0.148 mmol) of $\text{LaCl}_3\cdot 7\text{H}_2\text{O}$, 30.0 mg (0.152 mmol) of $\text{phen}\cdot\text{H}_2\text{O}$ and 53.0 mg (0.308 mmol) of H_2chdc were mixed in a glass vial and dissolved in the mixture of 7.5 mL of DMF and 1.5 mL of water. Then, the obtained solution was closed by a screw cap and heated at 80 °C for 2 days. The formed white precipitate was filtered off, washed with DMF and dried in air. A single crystal suitable for SCXRD was taken directly from the mother liquor before filtration. Yield: 33.5 mg (44%). IR spectrum (KBr, cm^{-1}) main bands: 3441 (m, br, $\nu\text{O-H}$); 2928 (m, $\nu\text{Csp}^3\text{-H}$); 2857 (m, $\nu\text{Csp}^3\text{-H}$); 1674 (w, $\nu\text{CO}_{\text{DMF}}$); 1606, 1580 and 1551 (m, $\nu\text{COO}_{\text{as}}$); 1410 (m, νCOO_{s}). Elemental analysis data for the sample **1'** after the filtration of **1** and its storage (%), calculated for $\text{La}_2(\text{C}_3\text{H}_7\text{NO})_{1.5}(\text{H}_2\text{O})_{0.5}(\text{C}_8\text{H}_{10}\text{O}_4)_3$: C, 37.7; H, 4.6; N, 2.3. Found: C, 37.9; H, 4.7; N, 2.5. TG data: 12% weight loss at 280 °C. Calculated for $1.5\text{DMF}+0.5\text{H}_2\text{O}$: 13%.

Synthesis of 2_{Ce} . Amounts of 43.0 mg (0.099 mmol) of $\text{Ce}(\text{NO}_3)_3\cdot 6\text{H}_2\text{O}$, 20.0 mg (0.101 mmol) of $\text{phen}\cdot\text{H}_2\text{O}$ and 26.0 mg (0.151 mmol) of H_2chdc were mixed in a glass vial and dissolved in the mixture of 1.2 mL of DMF and 0.8 mL of water. Then, the obtained solution was closed by a screw cap and heated at 80 °C for 2 days. The formed yellow precipitate was filtered off, washed with DMF and dried in air. A single crystal suitable for SCXRD was taken directly from the mother liquor before filtration. Yield:

16.3 mg (27%). IR spectrum (KBr, cm^{-1}) main bands: 3440 (w, br, $\nu\text{O-H}$); 3073 and 3059 (w, $\nu\text{Csp}^2\text{-H}$); 3012 and 2998 (w, $\nu\text{Csp}^2\text{-H}$); 2934 (m, $\nu\text{Csp}^3\text{-H}$); 2858 (m, $\nu\text{Csp}^3\text{-H}$); 1685 (s, $\nu\text{CO}_{\text{DMF}}$); 1586 (s, $\nu\text{COO}_{\text{as}}$); 1411 (s, νCOO_{s}). Elemental analysis data (%), calculated for $[\text{Ce}_2(\text{C}_{12}\text{H}_8\text{N}_2)_2(\text{C}_8\text{H}_{10}\text{O}_4)_3] \cdot 0.75\text{C}_3\text{H}_7\text{NO} \cdot \text{H}_2\text{O}$: C, 49.3; H, 4.4; N, 5.4. Found: C, 49.4; H, 4.5; N, 5.6. TG data: 5% weight loss until 400 °C. Calculated for 0.75DMF+H₂O: 6%.

Synthesis of **2Pr**, **2Nd** and **2Sm** was carried out analogously to the synthesis of **2Ce**, except for changing the cerium nitrate to the corresponding amounts of $\text{PrCl}_3 \cdot 7\text{H}_2\text{O}$, $\text{NdCl}_3 \cdot 7\text{H}_2\text{O}$ or $\text{SmCl}_3 \cdot 6\text{H}_2\text{O}$ and reducing the reaction time to 20 h.

2Pr. Yield of greenish precipitate: 15.3 mg (26%). IR spectrum (KBr, cm^{-1}) main bands: 3433 (w, br, $\nu\text{O-H}$); 3072 and 3058 (w, $\nu\text{Csp}^2\text{-H}$); 3009 and 2996 (w, $\nu\text{Csp}^2\text{-H}$); 2929 (m, $\nu\text{Csp}^3\text{-H}$); 2856 (m, $\nu\text{Csp}^3\text{-H}$); 1685 (s, $\nu\text{CO}_{\text{DMF}}$); 1586 (s, $\nu\text{COO}_{\text{as}}$); 1410 (s, νCOO_{s}). Elemental analysis data (%), calculated for $[\text{Pr}_2(\text{C}_{12}\text{H}_8\text{N}_2)_2(\text{C}_8\text{H}_{10}\text{O}_4)_3] \cdot 0.75\text{C}_3\text{H}_7\text{NO} \cdot \text{H}_2\text{O}$: C, 49.2; H, 4.4; N, 5.3. Found: C, 49.1; H, 4.4; N, 5.4. TG data: 4.5% weight loss until 430 °C. Calculated for 0.75DMF+H₂O: 6%.

2Nd. Yield of pinkish-blue precipitate: 15.0 mg (25%). IR spectrum (KBr, cm^{-1}) main bands: 3429 (w, br, $\nu\text{O-H}$); 3074 and 3059 (w, $\nu\text{Csp}^2\text{-H}$); 3011 and 2998 (w, $\nu\text{Csp}^2\text{-H}$); 2929 (m, $\nu\text{Csp}^3\text{-H}$); 2856 (m, $\nu\text{Csp}^3\text{-H}$); 1685 (s, $\nu\text{CO}_{\text{DMF}}$); 1585 (s, $\nu\text{COO}_{\text{as}}$); 1410 (s, νCOO_{s}). Elemental analysis data (%), calculated for $[\text{Nd}_2(\text{C}_{12}\text{H}_8\text{N}_2)_2(\text{C}_8\text{H}_{10}\text{O}_4)_3] \cdot 0.75\text{C}_3\text{H}_7\text{NO} \cdot 0.5\text{H}_2\text{O}$: C, 49.3; H, 4.3; N, 5.4. Found: C, 49.2; H, 4.4; N, 5.3. TG data: 4% weight loss until 440 °C. Calculated for 0.75DMF+0.5H₂O: 5%.

2Sm. Yield of white precipitate: 17.4 mg (29%). IR spectrum (KBr, cm^{-1}) main bands: 3443 (w, br, $\nu\text{O-H}$); 3076 and 3060 (w, $\nu\text{Csp}^2\text{-H}$); 3011 and 2998 (w, $\nu\text{Csp}^2\text{-H}$); 2929 (m, $\nu\text{Csp}^3\text{-H}$); 2856 (m, $\nu\text{Csp}^3\text{-H}$); 1685 (s, $\nu\text{CO}_{\text{DMF}}$); 1588 (s, $\nu\text{COO}_{\text{as}}$); 1413 (s, νCOO_{s}). Elemental analysis data (%), calculated for $[\text{Sm}_2(\text{C}_{12}\text{H}_8\text{N}_2)_2(\text{C}_8\text{H}_{10}\text{O}_4)_3] \cdot 0.75\text{C}_3\text{H}_7\text{NO}$: C, 49.2; H, 4.2; N, 5.4. Found: C, 49.0; H, 4.3; N, 5.3. TG data: 4% weight loss until 450 °C. Calculated for 0.75DMF: 4.5%.

Synthesis of **3**. Amounts of 38.0 mg (0.101 mmol) of $\text{NdCl}_3 \cdot 7\text{H}_2\text{O}$, 20.0 mg (0.101 mmol) of phen·H₂O and 34.5 mg (0.201 mmol) of H₂chdc were mixed in a glass vial and dissolved in 5.0 mL of DMF. Then, the obtained solution was closed by a screw cap and heated at 110 °C for 4 h. For performing PXRD, the resulting white precipitate was filtered off, washed by DMF and dried in air. Due to a weak diffraction from the obtained single crystals, for performing SCXRD analysis, mother liquor was replaced by pure DMF and then crystals of **3** were carefully stored in this form until synchrotron working trip. Yield: less than 10%.

3.4. Single-Crystal X-ray Diffraction Details

Diffraction data for single crystals of **1** and **2Ln** were collected on an automated Agilent Xcalibur diffractometer equipped with an area AtlasS2 detector (graphite monochromator, $\lambda(\text{MoK}\alpha) = 0.71073 \text{ \AA}$). Integration, absorption correction and determination of unit cell parameters were performed using the CrysAlisPro program package [75]. The structures were solved by the dual-space algorithm (SHELXT [76]) and refined by the full-matrix least-squares technique (SHELXL [77]) in the anisotropic approximation (except hydrogen atoms). Positions of hydrogen atoms of organic ligands were calculated geometrically and refined in the riding model. Diffraction data for single crystals of **3** were obtained on the 'Belok' beamline [78,79] ($\lambda = 0.745 \text{ \AA}$) of the National Research Center 'Kurchatov Institute' (Moscow, Russian Federation) using a Rayonix SX165 CCD detector. The data were indexed, integrated and scaled, and absorption correction was applied using the XDS program package [80]. The crystallographic data and details of the structure refinements are summarized in Tables S1 and S2.

4. Conclusions

To summarize, six new metal–organic frameworks based on early lanthanide(III) cations and *trans*-1,4-cyclohexanedicarboxylic acid (H₂chdc) were synthesized and structurally characterized. All the compounds possess three-dimensional coordination lattices.

However, a lanthanide contraction appears to provide a significant composition difference between lanthanum-based $[\text{La}_2(\text{H}_2\text{O})_4(\text{chdc})_3]$ with $\text{CN}(\text{La}^{3+}) = 10$ and lanthanide-based $[\text{Ln}_2(\text{phen})_2(\text{chdc})_3]$ frameworks with $\text{CN}(\text{Ln}^{3+}) = 9$, further resulting in a change in the main structural motif from one-dimensional metal–carboxylate chains to separate binuclear carboxylate building units. A variation of synthetic conditions gave two topological isomers of the $[\text{Nd}_2(\text{phen})_2(\text{chdc})_3]$ coordination framework, bearing primitive cubic **pcu** topology or rare hexagonal helical **snz** topologies. Luminescent measurements revealed a strong and nonmonotonous tuning of luminescence color for the compound $[\text{Sm}_2(\text{phen})_2(\text{chdc})_3] \cdot 0.75\text{DMF}$, while excitation wavelength varied, with an emission color change from pinkish red at $\lambda_{\text{ex}} = 340$ nm to white at $\lambda_{\text{ex}} = 400$ nm and then to yellow at lower excitation energies. Such behavior represents a rare example of both a white-light emitter and highly tunable luminophore based on a single lanthanide ion.

Supplementary Materials: The following supporting information can be downloaded at: <https://www.mdpi.com/article/10.3390/inorganics10100163/s1>, Table S1: Single-crystal XRD experiment and refinement details for **1**, **2_{Ce}**, **2_{Pr}**; Table S2: Single-crystal XRD experiment and refinement details for **2_{Nd}**, **2_{Sm}**, **3**; Figure S1: Experimental (black) and theoretical (red) PXRD patterns for **2_{Ce}**; Figure S2: Experimental (black) and theoretical (red) PXRD patterns for **2_{Pr}**; Figure S3: Experimental (black) and theoretical (red) PXRD patterns for **2_{Nd}**; Figure S4: Experimental (black) and theoretical (red) PXRD patterns for **2_{Sm}**; Figure S5: PXRD patterns for **2_{Pr}** temperature- and time-screening syntheses; Figure S6: PXRD patterns for **2_{Sm}** temperature- and time-screening syntheses; Figure S7: Coordination modes of $(k^2, k^1; k^2, k^1)$ -chdc ligand (**a**) and $(k^2; k^2)$ -chdc ligand (**b**); Figure S8: Space-filling representation of channels in the coordination framework of **1**; Figure S9: Experimental (black) PXRD pattern for **1'** and theoretical (red) one for **1** (a). View along *c* crystallographic axis in **1** (b); Figure S10: TGA pattern and relative dm/dT curve for the sample **1'**; Table S3: Selected bond lengths in **2_{Ln}** and **3**; Figure S11: Infrared spectra for **1'** and **2_{Ln}**; Table S4: Details on TG decomposition steps of **1'** and **2_{Ln}**; Figure S12: Excitation (red) spectrum for **2_{Nd}** at $\lambda_{\text{em}} = 1077$ nm and emission (black) spectrum for **2_{Nd}** at $\lambda_{\text{ex}} = 804$ nm; Figure S13: Excitation spectrum for **2_{Sm}** at $\lambda_{\text{em}} = 580$ nm.

Author Contributions: P.A.D.: Conceptualization, methodology, validation, investigation, writing—original draft preparation, visualization; A.A.R.: methodology, validation, investigation; V.P.F.—resources, writing—review and editing, project administration, funding acquisition. All authors have read and agreed to the published version of the manuscript.

Funding: This work was supported by the Ministry of Science and Higher Education of the Russian Federation (Agreement No. 075-15-2022-263). The experiments were performed using large-scale research facilities “EXAFS spectroscopy beamline”. Analytical services were provided under projects No. 121031700321-3 and 121031700313-8.

Data Availability Statement: CCDC 2190414–2190419 contains supplementary crystallographic data for this paper. These data can be obtained free of charge from The Cambridge Crystallographic Data Center [81].

Conflicts of Interest: The authors declare no conflict of interest.

References

1. Lu, W.; Wei, Z.; Gu, Z.-Y.; Liu, T.-F.; Park, J.; Park, J.; Tian, J.; Zhang, M.; Zhang, Q.; Gentle, T., III; et al. Tuning the structure and function of metal–organic frameworks via linker design. *Chem. Soc. Rev.* **2014**, *43*, 5561–5593. [CrossRef]
2. Feng, L.; Wang, K.-Y.; Lv, X.-L.; Yan, T.-H.; Zhou, H.-C. Hierarchically porous metal–organic frameworks: Synthetic strategies and applications. *Natl. Sci. Rev.* **2020**, *7*, 1743–1758. [CrossRef]
3. Li, X.; Wang, J.; Bai, N.; Zhang, X.; Han, X.; Da Silva, I.; Morris, C.G.; Xu, S.; Wilary, D.M.; Sun, Y.; et al. Refinement of pore size at sub-angstrom precision in robust metal–organic frameworks for separation of xylenes. *Nat. Commun.* **2020**, *11*, 4280. [CrossRef]
4. Yin, W.; Tao, C.; Wang, F.; Huang, J.; Qu, T.; Wang, J. Tuning optical properties of MOF-based thin films by changing the ligands of MOFs. *Sci. China Mater.* **2018**, *61*, 391–400. [CrossRef]
5. Wei, R.; Gaggioli, A.C.; Li, G.; Islamoglu, T.; Zhang, Z.; Yu, P.; Farha, O.K.; Cramer, C.J.; Gagliardi, L.; Yang, D.; et al. Tuning the Properties of Zr_6O_8 Nodes in the Metal Organic Framework UiO-66 by Selection of Node-Bound Ligands and Linkers. *Chem. Mater.* **2019**, *31*, 1655–1663. [CrossRef]
6. Kovalenko, K.A.; Potapov, A.S.; Fedin, V.P. Micro- and mesoporous metal-organic coordination polymers for the separation of hydrocarbons. *Russ. Chem. Rev.* **2022**, *91*, 1–31. [CrossRef]

7. Horike, S.; Shimomura, S.; Kitagawa, S. Soft porous crystals. *Nat. Chem.* **2009**, *1*, 695–704. [[CrossRef](#)]
8. Aljammal, N.; Jabbour, C.; Chaemchuen, S.; Juzsakova, T.; Verpoort, F. Flexibility in Metal–Organic Frameworks: A Basic Understanding. *Catalysts* **2019**, *9*, 512. [[CrossRef](#)]
9. Liu, Z.; Zhang, L.; Sun, D. Stimuli-responsive structural changes in metal–organic frameworks. *Chem. Commun.* **2020**, *56*, 9416–9432. [[CrossRef](#)]
10. Grebenyuk, D.; Zobel, M.; Polentarutti, M.; Ungur, L.; Kendin, M.; Zakharov, K.; Degtyarenko, P.; Vasiliev, A.; Tsymbarenko, D. A Family of Lanthanide Hydroxo Carboxylates with 1D Polymeric Topology and Ln₄ Butterfly Core Exhibits Switchable Supramolecular Arrangement. *Inorg. Chem.* **2021**, *60*, 8049–8061. [[CrossRef](#)]
11. Makal, T.A.; Yakovenko, A.A.; Zhou, H.-C. Isomerism in Metal–Organic Frameworks: “Framework Isomers”. *J. Phys. Chem. Lett.* **2011**, *2*, 1682–1689. [[CrossRef](#)]
12. Widmer, R.N.; Lampronti, G.I.; Chibani, S.; Wilson, C.W.; Anzellini, S.; Farsang, S.; Kleppe, A.K.; Casati, N.P.M.; MacLeod, S.G.; Redfern, S.A.T.; et al. Rich Polymorphism of a Metal–Organic Framework in Pressure–Temperature Space. *J. Am. Chem. Soc.* **2019**, *141*, 9330–9337. [[CrossRef](#)]
13. Dubskikh, V.A.; Lysova, A.A.; Samsonenko, D.G.; Dybtsev, D.N.; Fedin, V.P. Topological polymorphism and temperature-driven topotactic transitions of metal–organic coordination polymers. *CrystEngComm* **2020**, *22*, 6295–6301. [[CrossRef](#)]
14. Bueken, B.; Van Velthoven, N.; Krajnc, A.; Smolders, S.; Taulelle, F.; Mellot-Draznieks, C.; Mali, G.; Bennett, T.D.; De Vos, D. Tackling the Defect Conundrum in UiO-66: A Mixed-Linker Approach to Engineering Missing Linker Defects. *Chem. Mater.* **2017**, *29*, 10478–10486. [[CrossRef](#)]
15. Demakov, P.A.; Sapchenko, S.A.; Samsonenko, D.G.; Dybtsev, D.N.; Fedin, V.P. Coordination polymers based on zinc(II) and manganese(II) with 1,4-cyclohexanedicarboxylic acid. *Russ. Chem. Bull.* **2018**, *67*, 490–496. [[CrossRef](#)]
16. Reinsch, H.; Homburg, T.; Heidenreich, N.; Fröhlich, D.; Henninger, S.; Wark, M.; Stock, N. Green Synthesis of a New Al-MOF Based on the Aliphatic Linker Mesaconic Acid: Structure, Properties and In Situ Crystallisation Studies of Al-MIL-68-Mes. *Chem. Eur. J.* **2018**, *24*, 2173–2181. [[CrossRef](#)]
17. Macreadie, L.K.; Mensforth, E.J.; Babarao, R.; Konstas, K.; Telfer, S.G.; Doherty, C.M.; Tsanaktsidis, J.; Batten, S.R.; Hill, M.R. CUB-5: A Contoured Aliphatic Pore Environment in a Cubic Framework with Potential for Benzene Separation Applications. *J. Am. Chem. Soc.* **2019**, *141*, 3828–3832. [[CrossRef](#)]
18. Llabres-Campaner, P.J.; Pitarch-Jarque, J.; Ballesteros-Garrido, R.; Abarca, B.; Ballesteros, R.; García-España, E. Bicyclo[2.2.2]octane-1,4-dicarboxylic acid: Towards transparent metal-organic frameworks. *Dalton Trans.* **2017**, *46*, 7397–7402. [[CrossRef](#)]
19. Yin, J.; Yang, H.; Fei, H. Robust, Cationic Lead Halide Layered Materials with Efficient Broadband White-Light Emission. *Chem. Mater.* **2019**, *31*, 3909–3916. [[CrossRef](#)]
20. Zhao, S.-N.; Wang, G.; Poelman, D.; Van Der Voort, P. Luminescent Lanthanide MOFs: A Unique Platform for Chemical Sensing. *Materials* **2018**, *11*, 572. [[CrossRef](#)]
21. Saraci, F.; Quezada-Novoa, V.; Donnarumma, P.R.; Howarth, A.J. Rare-earth metal–organic frameworks: From structure to applications. *Chem. Soc. Rev.* **2020**, *49*, 7949–7977. [[CrossRef](#)]
22. Nguyen, T.N.; Eliseeva, S.V.; Gładysiak, A.; Petoud, S.; Stylianou, K.C. Design of lanthanide-based metal–organic frameworks with enhanced near-infrared emission. *J. Mater. Chem. A* **2020**, *8*, 10188–10192. [[CrossRef](#)]
23. Belousov, Y.A.; Drozdov, A.A.; Taydakov, I.V.; Marchetti, F.; Pettinari, R.; Pettinari, C. Lanthanide azolecarboxylate compounds: Structure, luminescent properties and applications. *Coord. Chem. Rev.* **2021**, *445*, 214084. [[CrossRef](#)]
24. Pan, M.; Liao, W.-M.; Yin, S.-Y.; Sun, S.-S.; Su, C.-Y. Single-Phase White-Light-Emitting and Photoluminescent Color-Tuning Coordination Assemblies. *Chem. Rev.* **2018**, *118*, 8889–8935. [[CrossRef](#)]
25. Igoa, F.; Peinado, G.; Suescun, L.; Kremer, C.; Torres, J. Design of a white-light emitting material based on a mixed-lanthanide metal organic framework. *J. Solid State Chem.* **2019**, *279*, 120925. [[CrossRef](#)]
26. Dong, Z.-P.; Zhao, F.; Zhang, L.; Liu, Z.-L.; Wang, Y.-Q. A white-light-emitting lanthanide metal–organic framework for luminescence turn-off sensing of MnO₄[−] and turn-on sensing of folic acid and construction of a “turn-on plus” system. *New J. Chem.* **2020**, *44*, 10239–10249. [[CrossRef](#)]
27. Sun, Z.; Khurshid, A.; Sohail, M.; Qiu, W.; Cao, D.; Su, S.-J. Encapsulation of Dyes in Luminescent Metal–Organic Frameworks for White Light Emitting Diodes. *Nanomaterials* **2021**, *11*, 2761. [[CrossRef](#)]
28. Demakov, P.A.; Ryadun, A.A.; Dorovatovskii, P.V.; Lazarenko, V.A.; Samsonenko, D.G.; Brylev, K.A.; Fedin, V.P.; Dybtsev, D.N. Intense multi-colored luminescence in a series of rare-earth metal–organic frameworks with aliphatic linkers. *Dalton Trans.* **2021**, *50*, 11899–11908. [[CrossRef](#)]
29. Wang, S.; Sun, B.; Sun, J.; Hao, X.; Li, X.; Zhou, C.; Su, Z. Lanthanide metal–organic frameworks based on planar π-conjugated ligands for white light emission, temperature and chemical sensing. *Dyes Pigm.* **2022**, *202*, 110256. [[CrossRef](#)]
30. Zehnder, R.A.; Jenkins, J.; Zeller, M.; Dempsey, C.; Kozimor, S.A.; Jackson, G.; Gilbert, K.; Smith, M. Conversion of lanthanide glutarate chlorides with interstitial THF into lanthanide glutarates with unprecedented topologies. *Inorg. Chim. Acta* **2018**, *471*, 502–512. [[CrossRef](#)]
31. Kumar, M.; Qiu, C.-Q.; Zareba, J.K.; Frontera, A.; Kaur Jassal, A.; Sahoo, S.C.; Liu, S.-J.; Nawaz Sheikh, H. Magnetic, luminescence, topological and theoretical studies of structurally diverse supramolecular lanthanide coordination polymers with flexible glutaric acid as a linker. *New J. Chem.* **2019**, *43*, 14546–14564. [[CrossRef](#)]

32. Long, D.-L.; Blake, A.J.; Champness, N.R.; Wilson, C.; Schröder, M. Unprecedented Seven- and Eight-Connected Lanthanide Coordination Networks. *Angew. Chem. Int. Ed.* **2001**, *40*, 2443–2447. [[CrossRef](#)]
33. Liu, L.; Wang, Y.; Lin, R.; Yao, Z.; Lin, Q.; Wang, L.; Zhang, Z.; Xiang, S. Two water-stable lanthanide metal–organic frameworks with oxygen-rich channels for fluorescence sensing of Fe(III) ions in aqueous solution. *Dalton Trans.* **2018**, *47*, 16190–16196. [[CrossRef](#)]
34. Pérez, J.M.; Rojas, S.; García-García, A.; Montes-Andrés, H.; Martínez, C.R.; Romero-Cano, M.S.; Choquesillo-Lazarte, D.; Abdelkader-Fernández, V.K.; Pérez-Mendoza, M.; Cepeda, J.; et al. Catalytic Performance and Electrophoretic Behavior of an Yttrium–Organic Framework Based on a Tricarboxylic Asymmetric Alkyne. *Inorg. Chem.* **2022**, *61*, 1377–1384. [[CrossRef](#)]
35. Lu, T.-Q.; Cheng, L.-T.; Wang, X.-T.; Chen, C.; Zheng, J.; Lu, D.-F.; Zheng, X.-Y. Lanthanide Metal–Organic Frameworks with High Chemical Stability as Multifunctional Materials: Cryogenic Magnetic Cooler and Luminescent Probe. *Cryst. Growth Des.* **2022**, *22*, 4917–4925. [[CrossRef](#)]
36. Liu, D.; Lu, K.; Poon, C.; Lin, W. Metal–Organic Frameworks as Sensory Materials and Imaging Agents. *Inorg. Chem.* **2014**, *53*, 1916–1924. [[CrossRef](#)]
37. Wang, H.-S. Metal–organic frameworks for biosensing and bioimaging applications. *Coord. Chem. Rev.* **2017**, *349*, 139–155. [[CrossRef](#)]
38. Sava Gallis, D.F.; Rohwer, L.E.S.; Rodriguez, M.A.; Barnhart-Dailey, M.C.; Butler, K.S.; Luk, T.S.; Timlin, J.A.; Chapman, K.W. Multifunctional, Tunable Metal–Organic Framework Materials Platform for Bioimaging Applications. *ACS Appl. Mater. Interfaces* **2017**, *9*, 22268–22277. [[CrossRef](#)]
39. Zhang, Q.; Li, J.; Zu, W.; Yang, H.; Wang, Y. One-pot synthesis of Eu-MOFs for bioimaging and drug delivery. *Drug Dev. Ind. Pharm.* **2021**, *47*, 1175–1182. [[CrossRef](#)]
40. Cui, R.; Sun, W.; Liu, M.; Shi, J.; Liu, Z. Near-Infrared Emissive Lanthanide Metal–Organic Frameworks for Targeted Biological Imaging and pH-Controlled Chemotherapy. *ACS Appl. Mater. Interfaces* **2021**, *13*, 59164–59173. [[CrossRef](#)]
41. Demakov, P.A.; Vasileva, A.A.; Volynkin, S.S.; Ryadun, A.A.; Samsonenko, D.G.; Fedin, V.P.; Dybtsev, D.N. Cinnamal Sensing and Luminescence Color Tuning in a Series of Rare-Earth Metal–Organic Frameworks with *Trans*-1,4-cyclohexanedicarboxylate. *Molecules* **2021**, *26*, 5145. [[CrossRef](#)]
42. Anderegg, G. Pyridinderivate als Komplexbildner VI. Reaktionsenthalpie und entropie bei der Bildung der Metallkomplexe von 1,10-Phenanthrolin und α, α' -Dipyridyl. *Helv. Chim. Acta* **1963**, *46*, 2813–2822. [[CrossRef](#)]
43. Bencini, A.; Lippolis, V. 1,10-Phenanthroline: A versatile building block for the construction of ligands for various purposes. *Coord. Chem. Rev.* **2010**, *254*, 2096–2180. [[CrossRef](#)]
44. Tan, X.-F.; Zhou, J.; Zou, H.-H.; Fu, L.; Tang, Q.; Wang, P. A series of lanthanide glutarates: Lanthanide contraction effect on crystal frameworks of lanthanide glutarates. *RSC Adv.* **2017**, *7*, 17934–17940. [[CrossRef](#)]
45. Demakov, P.A.; Sapchenko, S.A.; Samsonenko, D.G.; Dybtsev, D.N.; Fedin, V.P. Gadolinium Break in a Series of Three-Dimensional *trans*-1,4-Cyclohexane Dicarboxylates of Rare Earth Elements. *J. Struct. Chem.* **2019**, *60*, 815–822. [[CrossRef](#)]
46. Spek, A.L. Single-crystal structure validation with the program PLATON. *J. Appl. Crystallogr.* **2003**, *36*, 7–13. [[CrossRef](#)]
47. Liu, G.-Z.; Xin, L.-Y.; Wang, L.-Y. Ancillary ligand-mediated syntheses and fluorescence properties of zinc(II) complexes based on flexible benzene dicarboxylic acid. *CrystEngComm* **2011**, *13*, 3013–3020. [[CrossRef](#)]
48. Manna, P.; Tripuramallu, B.K.; Bommakanti, S.; Das, S.K. Synthesis, characterization and magnetism of metal–organic compounds: Role of the positions of the coordinating groups of a meso-flexible ligand in placing anisotropy to exhibit spin-canting behaviour. *Dalton Trans.* **2015**, *44*, 2852–2864. [[CrossRef](#)]
49. Singh, S.S. Infrared Spectra of 1:10 Phenanthroline and its Addition Compounds with Antimony Trichloride and Antimony Pentachloride. *Z. Nat. A* **1969**, *24*, 2015–2016. [[CrossRef](#)]
50. Reiher, M.; Brehm, G.; Schneider, S. Assignment of Vibrational Spectra of 1,10-Phenanthroline by Comparison with Frequencies and Raman Intensities from Density Functional Calculations. *J. Phys. Chem. A* **2004**, *108*, 734–742. [[CrossRef](#)]
51. Li, C.-T.; Zhao, Y.-F.; Hu, H.-M.; Zhao, H.; Wang, X.; Xue, G. Lanthanide coordination frameworks constructed from 3,3',4,4'-diphenylsulfonetetracarboxylic and 1,10-phenanthroline: Synthesis, crystal structures and luminescence properties. *Dalton Trans.* **2016**, *45*, 15436–15444. [[CrossRef](#)]
52. Zheng, K.; Liu, Z.-Q.; Huang, Y.; Chen, F.; Zeng, C.-H.; Zhong, S.; Ng, S.W. Highly luminescent Ln-MOFs based on 1,3-adamantanedi-acetic acid as bifunctional sensor. *Sens. Actuators B Chem.* **2018**, *257*, 705–713. [[CrossRef](#)]
53. Feng, X.; Shang, Y.; Zhang, H.; Li, R.; Wang, W.; Zhang, D.; Wang, L.; Li, Z. Enhanced luminescence and tunable magnetic properties of lanthanide coordination polymers based on fluorine substitution and phenanthroline ligand. *RSC Adv.* **2019**, *9*, 16328–16338. [[CrossRef](#)]
54. Liang, Y.-Y.; Xue, L.-L.; Hu, H.-M.; Zheng, L.-N.; Wang, X.; Xue, G. Syntheses, structures, fluorescence sensing properties and white-light emission of lanthanide coordination polymers assembled from imidazophenanthroline derivative and isophthalate ligands. *J. Solid State Chem.* **2019**, *276*, 6–18. [[CrossRef](#)]
55. An, R.; Wang, X.; Hu, H.-M.; Zhao, Z.; Bai, C.; Xue, G. Controllable synthesis of four series of lanthanide coordination polymers: Synthesis, structures, luminescent and magnetic properties. *CrystEngComm* **2015**, *17*, 8289–8299. [[CrossRef](#)]
56. Litvinova, Y.M.; Gayfulin, Y.M.; Brylev, K.A.; Piryazev, D.A.; Van Leusen, J.; Kögerler, P.; Mironov, Y.V. Metal–organic frameworks with solvent-free lanthanide coordination environments: Synthesis from aqueous ethanol solutions. *CrystEngComm* **2020**, *22*, 7935–7943. [[CrossRef](#)]

57. Roitershtein, D.M.; Puntus, L.N.; Varaksina, E.A.; Taidakov, I.V.; Lysenko, K.A. Lanthanide Coordination Polymers Based on Dicyanamide Ligand. *Russ. J. Coord. Chem.* **2020**, *46*, 15–22. [[CrossRef](#)]
58. But, S.; Lis, S.; Van Deun, R.; Parac-Vogt, T.N.; Görrler-Walrand, C.; Binnemans, K. Spectroscopic properties of neodymium(III)-containing polyoxometalates in aqueous solution. *Spectrochim. Acta A Mol. Biomol. Spectrosc.* **2005**, *62*, 478–482. [[CrossRef](#)]
59. Zapata-Lizama, M.; Hermosilla-Ibáñez, P.; Venegas-Yazigi, D.; Espallargas, G.M.; Maia, L.J.Q.; Gasparotto, G.; De Santana, R.C.; Cañón-Mancisidor, W. A systematic study of the optical properties of mononuclear hybrid organo–inorganic lanthanoid complexes. *Inorg. Chem. Front.* **2020**, *7*, 3049–3062. [[CrossRef](#)]
60. Metlina, D.A.; Metlin, M.T.; Ambrozevich, S.A.; Selyukov, A.S.; Datskevich, N.P.; Aminev, D.F.; Goryachii, D.O.; Lyssenko, K.A.; Pavlov, A.A.; Dmitrienko, A.O.; et al. Bright NIR-luminescent Nd³⁺ complexes with pyrazole-substituted 1,3-diketones demonstrated an unusual spectral lines branching ratios. *Dyes Pigm.* **2020**, *181*, 108558. [[CrossRef](#)]
61. Li, X.; Zhang, Y.-B.; Zou, Y.-Q. Hydrothermal synthesis, crystal structure, and luminescence of lanthanide(III) coordination polymers with tetrafluorosuccinate and 1,10-phenanthroline. *J. Mol. Struct.* **2009**, *919*, 277–283. [[CrossRef](#)]
62. Wang, X.-J.; Jiang, Z.-G.; Chen, J.; Feng, Y.-L. Lanthanide complexes with disulfide ligand generated in situ: Syntheses, crystal structures and fluorescent properties. *Inorg. Chim. Acta* **2011**, *373*, 270–275. [[CrossRef](#)]
63. Zhao, J.; Zhu, G.-H.; Xie, L.-Q.; Wu, Y.-S.; Wu, H.-L.; Zhou, A.-J.; Wu, Z.-Y.; Wang, J.; Chen, Y.-C.; Tong, M.-L. Magnetic and luminescent properties of lanthanide coordination polymers with asymmetric biphenyl-3,2',5'-tricarboxylate. *Dalton Trans.* **2015**, *44*, 14424–14435. [[CrossRef](#)]
64. Song, S.; Li, X.; Zhang, Y.-H.; Huo, R.; Ma, D. White light emission by a lanthanide doped Sm(III) framework constructed from 4-sulfobenzoate and 1H-imidazo[4,5-f][1,10]-phenanthroline. *Dalton Trans.* **2014**, *43*, 5974–5977. [[CrossRef](#)]
65. Xu, B.; Chen, Q.; Hu, H.-M.; An, R.; Wang, X.; Xue, G. Hydrothermal Syntheses, Crystal Structures, and Luminescence Properties of Lanthanide-Based Coordination Polymers Constructed by Sulfonate Functionalized Imidazophenanthroline Derivative Ligand. *Cryst. Growth Des.* **2015**, *15*, 2318–2329. [[CrossRef](#)]
66. Li, J.-J.; Fan, T.-T.; Qu, X.-L.; Han, H.-L.; Li, X. Temperature-induced 1D lanthanide polymeric frameworks based on Ln_n (n = 2, 2, 4, 6) cores: Synthesis, crystal structures and luminescence properties. *Dalton Trans.* **2016**, *45*, 2924–2935. [[CrossRef](#)]
67. Zhang, Y.-H.; Li, X.; Song, S.; Yang, H.-Y.; Ma, D.; Liu, Y.-H. Lanthanide coordination frameworks: Crystal structure, down- and up-conversion luminescence and white light emission. *CrystEngComm* **2014**, *16*, 8390–8397. [[CrossRef](#)]
68. Smirnova, K.S.; Ivanova, E.A.; Sukhikh, T.S.; Pozdnyakov, I.P.; Dotsenko, V.V.; Lider, E.V. Luminescent properties of Ln(III) complexes with 2-[(phenylamino)methylene]-5,5-dimethyl-cyclohexane-1,3-dione as an antenna. *Inorg. Chim. Acta* **2021**, *525*, 120490. [[CrossRef](#)]
69. Li, H.; Liu, H.-B.; Tao, X.-M.; Su, J.; Ning, P.-F.; Xu, X.-F.; Zhou, Y.; Gu, W.; Liu, X. Novel single component tri-rare-earth emitting MOF for warm white light LEDs. *Dalton Trans.* **2018**, *47*, 8427–8433. [[CrossRef](#)]
70. Ivanova, A.A.; Gontcharenko, V.E.; Lunev, A.M.; Sidoruk, A.V.; Arkhipov, I.A.; Taydakov, I.V.; Belousov, Y.A. New Carboxylate Anionic Sm-MOF: Synthesis, Structure and Effect of the Isomorphic Substitution of Sm³⁺ with Gd³⁺ and Tb³⁺ Ions on the Luminescent Properties. *Inorganics* **2022**, *10*, 104. [[CrossRef](#)]
71. Zhang, Y.-H.; Li, X.; Song, S. White light emission based on a single component Sm(III) framework and a two component Eu(III)-doped Gd(III) framework constructed from 2,2'-diphenyl dicarboxylate and 1H-imidazo[4,5-f][1,10]-phenanthroline. *Chem. Commun.* **2013**, *49*, 10397–10399. [[CrossRef](#)]
72. Luo, L.-L.; Qu, X.-L.; Li, Z.; Li, X.; Sun, H.-L. Isostructural lanthanide-based metal–organic frameworks: Structure, photoluminescence and magnetic properties. *Dalton Trans.* **2018**, *47*, 925–934. [[CrossRef](#)]
73. Xu, Q.-W.; Dong, G.; Cui, R.; Li, X. 3D lanthanide-coordination frameworks constructed by a ternary mixed-ligand: Crystal structure, luminescence and luminescence sensing. *CrystEngComm* **2020**, *22*, 740–750. [[CrossRef](#)]
74. Han, Y.; Yan, P.; Sun, J.; An, G.; Yao, X.; Li, Y.; Li, G. Luminescence and white-light emitting luminescent sensor of tetrafluoroterephthalate-lanthanide metal–organic frameworks. *Dalton Trans.* **2017**, *46*, 4642–4653. [[CrossRef](#)]
75. *CrysAlisPro 1.171.38.46*; Rigaku Oxford Diffraction: The Woodlands, TX, USA, 2015.
76. Sheldrick, G.M. SHELXT—Integrated space-group and crystal-structure determination. *Acta Crystallogr.* **2015**, *A71*, 3–8. [[CrossRef](#)]
77. Sheldrick, G.M. Crystal structure refinement with SHELXL. *Acta Crystallogr.* **2015**, *C71*, 3–8.
78. Svetogorov, R.D.; Dorovatovskii, P.V.; Lazarenko, V.A. Belok/XSA Diffraction Beamline for Studying Crystalline Samples at Kurchatov Synchrotron Radiation Source. *Cryst. Res. Technol.* **2020**, *55*, 1900184. [[CrossRef](#)]
79. Lazarenko, V.A.; Dorovatovskii, P.V.; Zubavichus, Y.V.; Burlov, A.S.; Koshchienko, Y.V.; Vlasenko, V.G.; Khrustalev, V.N. High-Throughput Small-Molecule Crystallography at the 'Belok' Beamline of the Kurchatov Synchrotron Radiation Source: Transition Metal Complexes with Azomethine Ligands as a Case Study. *Crystals* **2017**, *7*, 325. [[CrossRef](#)]
80. Kabsch, W. XDS. *Acta Crystallogr.* **2010**, *66*, 125–132. [[CrossRef](#)]
81. Cambridge Crystallographic Data Center (CCDC) Structure Search. Available online: <https://www.ccdc.cam.ac.uk/structures/> (accessed on 30 September 2022).